ELSEVIER

International Journal of Heat and Fluid Flow 19 (1998) 135–149

International Journal of HEAT AND FLUID FLOW

Turbulent budgets of natural convection in an infinite, differentially heated, vertical channel

T.A.M. Versteegh, F.T.M. Nieuwstadt *

J.M. Burgers Centre, Delft University of Technology, Rotterdamseweg 145, 2628 AL Delft, The Netherlands

Received 29 August 1997; accepted 25 October 1997

Abstract

A Direct Numerical Simulation (DNS) of natural convection flow in an infinite, differentially heated, vertical channel has been performed at four Rayleigh numbers varying from 5.4×10^5 to 5.0×10^6 for $\mathrm{Pr} = 0.709$. The attention will be focused on the turbulent Reynolds-stresses, fluxes, variances and their budgets. We will interpret the budgets in terms of the physical processes that determine this flow. In addition we have calculated the stresses and budgets based on the structures found from linear stability analysis of the laminar solution of this problem. The latter budgets will be compared with the budgets for fully developed turbulent flow, in order to estimate the influence of the large scale coherent structures on the budgets.

Keywords: Natural convection; Direct numerical simulation

Notation

B	buoyant production
C_2	two-point correlation
f_t	horizontal temperature flux
G	mean gradient production
g	gravitational acceleration
h	distance between the walls
L_x, L_y, L_z	geometry size in x-, y- and z-direction
N_x, N_y, N_z	number of gridpoints in x-, y- and z-direction
Nu	Nusselt number, $f_t h/\alpha\Delta T$
p'	fluctuating pressure
Pr	Prandtl number
R	rest term in turbulent budget
Ra	Rayleigh number, $\mathrm{Ra} = g\beta\Delta T h^3/\nu\alpha$
T_a, T_d, T_p	advective, diffusive, pressure transport in turbulent budget
T'	fluctuating temperature
T_0	reference temperature
$\bar{T}$	average temperature
u', v', w'	fluctuating velocities in x-, y- and z-direction
w_*	turbulent velocity scale
$\bar{W}$	average vertical velocity
x, y, z	wall-normal, spanwise and vertical coordinates

Greek

β	thermal exapansion coefficient
δ_{ij}	Kronecker delta
ΔT	temperature difference between the walls
Δ_x	grid size in x-direction
E	dissipation
ν	kinematic viscosity
α	thermal diffusivity
Φ	pressure–strain
Π	velocity–pressure gradient term

Subscript

max	maximum value
min	minimum value
B	buoyant part
R	rapid part
S	slow part
W	wall part
v_w	wall value
$\bar{}$	ensemble average over time and the homogeneous directions

1. Introduction

The investigation of turbulence is most conveniently made in simple flow configurations where the influence of various physical processes can be isolated and studied in detail. One of these geometries is the flow between two infinite walls, or 'plane channel'. Here, we consider such a geometry in the form of two vertical, infinite walls which are kept at different temperatures, i.e. one of the walls has a higher temperature with respect to the other. As a result of this temperature difference a natural convection flow develops and, if the temperature difference is sufficiently large, this flow becomes turbulent. This type of turbulent flow is interesting from an applied point of view, because it is representative of many practical heat

* Corresponding author. E-mail: t.niewstadt@wbmt.tubelft.nl.

0142-727X/98/$19.00
PII: S0142-727X(97)10018-2

transfer applications, such as the flow between double glazed windows or inside a hollow wall. Furthermore, the flow has links with single heated or cooled walls of which the applications are numerous. However, this flow is also interesting from a fundamental point of view, because unlike the more familiar case of convection above a horizontal wall, the production of turbulence by shear and buoyancy takes place in the same direction. Furthermore, the homogeneity in two directions ensures that no disturbing top/bottom, or sidewall effects are present.

We have studied the turbulent regime of this flow by means of DNS. With the help of DNS it is possible to study the details of turbulence. One of these details is the budget of turbulent quantities, such as Reynolds-stress components, heat fluxes and temperature variances. In principle one should also be able to obtain these second-order statistics from experiments; however, it is still a very difficult task to measure Reynolds stresses, fluxes and their budgets, especially in regions near the wall. Nevertheless, this wall region is important for the behaviour of the entire flow. Although LDA measurements have somewhat relieved the problem of measuring stresses, until now the only reliable sources of all terms in the Reynolds-budgets are DNS techniques. But even with the help of DNS-data, the calculation of second-order statistics involving all components such as production, transport and dissipation, is very elaborate, and only few papers give full information on these budgets. For instance, budgets in a standard channel flow have been published by Mansour et al. (1988).

Another advantage of DNS is that it allows us to compute terms which cannot be observed experimentally. An example is the pressure–strain term. Moreover, DNS makes it possible to study the individual contributions to the pressure–strain term separately. Information on these budgets can, for instance, be used for the development of advanced turbulence models. An example is the second-order closure modelling where a closure hypothesis has to be found for several terms in the budget equations of the second-order moments. These closure hypotheses can thus be tested with DNS data.

In natural convection flows one frequently finds large-scale flow motions and these also exist in the present flow. These large-scale motions are usually interpreted as remnants of the flow structures that appear during the onset of turbulence, i.e. as a result of linear instability of the laminar flow. In a separate study (Versteegh, 1998) we have performed this linear stability analysis and obtained the flow mode connected to the most unstable eigenvalue. Here we have computed the budgets for this linear instability mode. From a comparison with the turbulent budgets a first estimate can be made as to how much the turbulence budgets are influenced by large-scale flow motions that occur in transitional flow.

On the subject of stability in natural convection in vertical slots and channels, many studies have already been published. Batchelor (1954) – the earliest study that we know of – gave rough estimates for the critical Rayleigh number. Later experimental data by Elder (1965a, b) gave insight in the flow patterns that occur in a flow with viscous fluids. From the end of the sixties, when computer power gradually became available, to the end of the eighties, these, numerical studies about linear stability were published. Among these, we mention Elder (1966), Vest and Arpaci (1969), Korpela et al. (1973), Chait and Korpela (1989).

Despite the many experimental and numerical data on transitional flow, for many years no data were available for turbulent flow. Therefore, turbulence modelling for this type of flow is still dependent on models originally developed for shear flows (like channel or Couette flow). Ince and Launder (1989) used a low Reynolds number k–ϵ model to reproduce experimental data that were reported by D'afa alla (1988). Later DNS data gave another impulse to the turbulence modelling for this type of flow, and improvement was obtained by Boudjemadi et al. (1997) and Dol et al. (1997a).

During the last decade, experimental data on the turbulent regime of this flow were produced by the group of Betts. We have already mentioned D'afa alla (1988), but later D'afa alla and Betts (1990) and Betts and Bokhari (1996) presented new data, where the more recent data were generally of better quality than the earlier ones. All experiments were carried out for air in a vertical slot with aspect ratio of 28.6, with Ra varying from 8.23×10^5 to 1.43×10^6. Besides profiles of the average velocity and temperature, profiles of average stresses and fluxes were also produced by means of LDA.

Few DNS-data on natural convection in a differentially heated vertical channel exist. The first have been reported by Phillips (1996) for $\mathrm{Ra} = 5.75 \times 10^3$ and $\mathrm{Ra} = 1.60 \times 10^4$. Later, Boudjemadi et al. (1997) presented data for $\mathrm{Ra} = 10^5$ and $\mathrm{Ra} = 5.4 \times 10^5$. The latter also presented budgets on the turbulent regime.

Our aim is to give additional information on these budget data. In fact, our results differ in four aspects from the data published by Boudjemadi et al. (1997). First, the maximum Rayleigh number for our computations is about ten times higher ($\mathrm{Ra} = 5.0 \times 10^6$), which means that the turbulence level is significantly higher. Second, we are able to give more extended information about the budgets. Third, we will show the results in the light of the budgets of the first instability mode. Finally, our computational domain was considerably larger than used previously. We will show in this paper that this leads to somewhat different results.

To give an outline of this paper, first some theory is considered. Next, we present some results of the numerical simulations, in particular the profiles of the average velocity and temperature and of the non-zero Reynolds-stress components. Then, the turbulence budgets are considered in more detail. Finally, we end with some conclusions.

2. Theory

2.1. Governing equations

The geometry of our flow problem is illustrated in Fig. 1. We have taken the u-velocity and x-axis perpendicular to the walls, the v-velocity and y-axis in the span-wise direction (perpendicular to the plane of the figure) and finally the w-velocity and the z-axis in the vertical direction. Only in the latter direction is the average velocity non-zero.

The distance between the two walls (h) is used as a length scale and the temperature difference between the two walls

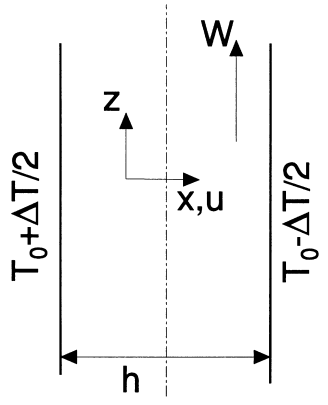

Fig. 1. Geometry of the two differentially heated, vertical walls.

(ΔT) as a temperature scale. The fluid has a kinematic viscosity (ν) and a kinematic diffusivity (α). The ratio of the two, defined as the Prandtl number ($\mathrm{Pr} = \nu/\alpha$) is taken to be equal to 0.709 (air). From the diffusivity and the length scale, we can derive a time-scale (h^2/α) and velocity scale (α/h). These scales are used to express the incompressible Boussinesq equations in the following dimensionless form:

$$\frac{\partial u_j}{\partial x_j} = 0,$$
$$\frac{\partial u_i}{\partial t} + \frac{\partial u_i u_j}{\partial x_j} = -\frac{\partial p}{\partial x_i} + \mathrm{RaPr}(T - T_0)\delta_{i3} + \mathrm{Pr}\frac{\partial^2 u_i}{\partial x_j^2},$$
$$\frac{\partial T}{\partial t} + \frac{\partial u_j T}{\partial x} = \frac{\partial^2 T}{\partial x_j^2}, \tag{1}$$

where δ_{ij} is the Kronecker delta and the Rayleigh number is defined as: $\mathrm{Ra} = g\beta\Delta T h^3/\nu\alpha$, with β the thermal expansion coefficient. The reference temperature (T_0) is the average temperature of the fluid.

For turbulent flow this is not a proper scaling. Therefore, the outer scaling proposed in Nieuwstadt and Versteegh (1997) and Versteegh (1998) is used in order to scale the turbulent budgets. Here, we only resume some important results.

Outside the near-wall region the appropriate scaling variables are h, f_t and $g\beta$, where the horizontal temperature flux (f_t) is constant in this flow, i.e. not a function of x. With these parameters a velocity scale can be defined as

$$w_* = (g\beta f_t h)^{\frac{1}{3}}. \tag{2}$$

Taking into account that we have used the velocity scale, α/h to non-dimensionalise Eq. (1) and the result found by Nieuwstadt and Versteegh (1997) that

$$\mathrm{Nu} = \frac{f_t h}{\alpha \Delta T} \sim \mathrm{Ra}^{\frac{1}{3}}, \tag{3}$$

we find, e.g., that all non-dimensional velocities should scale according to $\mathrm{Ra}^{4/9}$ and the temperature flux according to $\mathrm{Ra}^{1/3}$ (Fig. 2(a)).

2.2. Linear stability

For the case of laminar flow which occurs at small temperature differences, the set of equations (1) can be solved exactly (Batchelor, 1954). The result reads

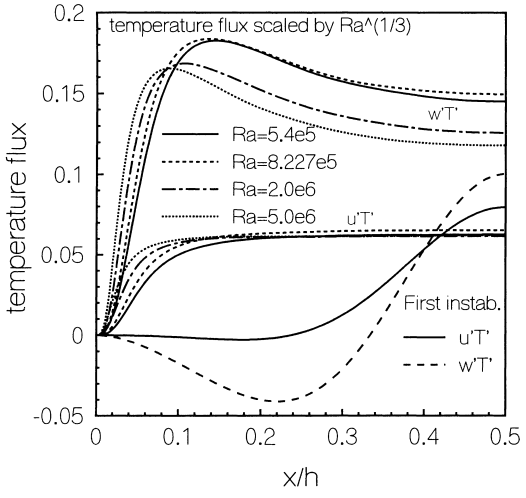

Fig. 2. Turbulent temperature fluxes scaled by $\mathrm{Ra}^{\frac{1}{3}}$ and the temperature flux of the first instability.

$$\overline{W}(x) = \frac{\mathrm{Ra}}{12}(2x^3 - 3x^2 + x), \qquad \overline{T}(x) = 0.5 - x, \tag{4}$$

where $\overline{W}$ and $\overline{T}$ are the laminar velocity and temperature profile.

In order to obtain the equations for linear stability analysis, small perturbations denoted with a prime are superposed on this laminar solution. Substitution in Eq. (1) and linearising leads to a set of linear equations for the perturbations, which are taken as only two-dimensional according to Squire's theorem,

$$\frac{\partial u_j'}{\partial x_j} = 0,$$
$$\frac{\partial u'}{\partial t} + \overline{W}\frac{\partial u'}{\partial z} = -\frac{\partial p'}{\partial x} + \mathrm{Pr}\left(\frac{\partial^2 u'}{\partial x^2} + \frac{\partial^2 u'}{\partial z^2}\right),$$
$$\frac{\partial w'}{\partial t} + u'\frac{\partial \overline{W}}{\partial x} + \overline{W}\frac{\partial w'}{\partial z} = -\frac{\partial p'}{\partial z} + \mathrm{RaPr}T' + \mathrm{Pr}\left(\frac{\partial^2 w'}{\partial x^2} + \frac{\partial^2 w'}{\partial z^2}\right),$$
$$\frac{\partial T'}{\partial t} + u'\frac{\partial \overline{T}}{\partial x} = \frac{\partial^2 T'}{\partial x^2} + \frac{\partial^2 T'}{\partial z^2}. \tag{5}$$

These linear stability equations have been solved with aid of a spectral method, using Chebyshev polynomials. For further information about the equations, solution methods and solutions we refer to Versteegh (1998), Boomkamp et al. (1997), Drazin and Reid (1981) and Chait and Korpela (1989).

With this method, we have calculated the eigenfunctions that belong to the first instability mode and the critical Rayleigh number ($\mathrm{Ra_{cr}}$) above which this mode grows exponentially. Here we present the variances and fluxes from the eigenfunctions as well as their budgets. Since the first instability mode is two-dimensional, the $\overline{v'v'}$-stress and its budget is zero.

2.3. Reynolds stresses

In this presentation, we will focus our attention on the variances and fluxes, both for the first instability mode and for the turbulent flow. The Reynolds-stress equations have been derived in the usual manner by splitting the variables into an average part and a fluctuating part and by multiplying these fluctuations with the momentum equations for the fluctuating part. Finally we apply an averaging procedure on the stress equations both in time and in the two homogeneous directions. Average values are denoted with an overbar.

The equation for the average turbulent transport of vertical momentum in horizontal direction is expressed as the time change of $\overline{u'w'}$. This time change is zero because of quasi-stationarity. Hence.

$$0 = \underbrace{-\overline{u'u'}\frac{\partial \overline{W}}{\partial x}}_{G} \underbrace{- \frac{\partial}{\partial x}\Big(\overbrace{\overline{u'u'w'}}^{T_\alpha} + \overbrace{\overline{w'p'}}^{T_p} + \overbrace{Pr\frac{\partial \overline{u'w'}}{\partial x}}^{T_d}\Big)}_{T}$$
$$\underbrace{+\overline{p'\Big(\frac{\partial u'}{\partial z} + \frac{\partial w'}{\partial x}\Big)}}_{\Phi} + \underbrace{RaPr\overline{u'T'}}_{B} \underbrace{- 2Pr\overline{\frac{\partial u'}{\partial x_j}\frac{\partial w'}{\partial x_j}}}_{E}. \tag{6}$$

The three following equations describe the time change of $\overline{u'u'}$, $\overline{v'v'}$ and $\overline{w'w'}$, respectively. The sum of these equations is exactly twice the equation for the turbulent kinetic energy.

$$0 = \underbrace{-\frac{\partial}{\partial x}\Big(\overline{u'u'u'} + \overline{u'p'} + Pr\frac{\partial \overline{u'u'}}{\partial x}\Big)}_{T} + \underbrace{2\overline{p'\frac{\partial u'}{\partial x}}}_{\Phi} \underbrace{- 2Pr\overline{\frac{\partial u'}{\partial x_j}\frac{\partial u'}{\partial x_j}}}_{E}, \tag{7}$$

$$0 = -\underbrace{\frac{\partial}{\partial x}(\overline{u'v'v'} + Pr\frac{\partial \overline{v'v'}}{\partial x})}_{T} + \underbrace{2\overline{p'\frac{\partial v'}{\partial y}}}_{\Phi} - \underbrace{2Pr\overline{\frac{\partial v'}{\partial x_j}\frac{\partial v'}{\partial x_j}}}_{E}, \tag{8}$$

$$0 = -\underbrace{2\overline{u'w'}\frac{\partial \overline{W}}{\partial x}}_{G} - \underbrace{\frac{\partial}{\partial x}(\overline{u'w'w'} + Pr\frac{\partial \overline{w'w'}}{\partial x})}_{T} + \underbrace{2\overline{p'\frac{\partial w'}{\partial z}}}_{\Phi} + \underbrace{2RaPr\overline{w'T'}}_{B} - \underbrace{2Pr\overline{\frac{\partial w'}{\partial x_j}\frac{\partial w'}{\partial x_j}}}_{E}. \tag{9}$$

In a same manner as for the $\overline{u'w'}$-budget, we can derive the equations for the horizontal and vertical temperature transport, $\overline{u'T'}$ and $\overline{w'T'}$ respectively. The results read as follows:

$$0 = -\underbrace{2\overline{u'u'}\frac{\partial \overline{T}}{\partial x}}_{G_T} - \underbrace{\frac{\partial}{\partial x}(\overline{u'u'T'} + \overline{T'p'} + Pr\frac{\partial \overline{u'T'}}{\partial x})}_{T} + \underbrace{\overline{p'\frac{\partial T'}{\partial x}}}_{\Phi} - \underbrace{(\frac{Pr-1}{Pr})\overline{T'\frac{\partial^2 u'}{\partial x_j^2}}}_{R} - \underbrace{2Pr\overline{\frac{\partial u'}{\partial x_j}\frac{\partial T'}{\partial x_j}}}_{E}, \tag{10}$$

$$0 = -\underbrace{\overbrace{\overline{u'w'}}^{G_T}\frac{\partial \overline{T}}{\partial x} - \overbrace{\overline{u'T'}}^{G_W}\frac{\partial \overline{W}}{\partial x}}_{G} - \underbrace{\frac{\partial}{\partial x}(\overline{u'w'T'} + Pr\frac{\partial \overline{w'T'}}{\partial x})}_{T} + \underbrace{\overline{p'\frac{\partial T'}{\partial z}}}_{\Phi} - \underbrace{(\frac{Pr-1}{Pr})\overline{T'\frac{\partial^2 w'}{\partial x_j^2}}}_{R} - \underbrace{2Pr\overline{\frac{\partial w'}{\partial x_j}\frac{\partial T'}{\partial x_j}}}_{E}. \tag{11}$$

Finally, the budget of the temperature variance equation is given by

$$0 = -\underbrace{2\overline{u'T'}\frac{\partial \overline{T}}{\partial x}}_{G_T} - \underbrace{\frac{\partial}{\partial x}(\overline{u'T'T'} + \frac{\partial \overline{T'T'}}{\partial x})}_{T} - \underbrace{2Pr\overline{\frac{\partial T'}{\partial x_j}\frac{\partial T'}{\partial x_j}}}_{E}. \tag{12}$$

In these equations the following terms can be distinguished: the mean gradient production term (G), the transport term (T), the pressure term (Φ), the buoyant term (B) and the dissipation term (E).

In the $\overline{u'T'}$- and $\overline{w'T'}$-budgets, an extra term arises from the fact that Pr $\neq 1$. This term will here be denoted as a rest term (R). For the temperature fluxes, there is more than one way to write down the combination of pressure transport, dissipation and the rest term. However, a general form of the equation can be written as

$$\underbrace{\frac{(a+bPr)}{(a+b)}\frac{\partial^2 \overline{u_i'T'}}{\partial x_j^2}}_{T_p}, \quad \underbrace{\frac{(a+bPr)}{(a+b)}\overline{\frac{\partial u_i'}{\partial x_j}\frac{\partial T'}{\partial x_j}}}_{E}, \quad \underbrace{\frac{(1-Pr)}{(a+b)}(a\overline{u'\frac{\partial^2 T'}{\partial x_j^2}} - b\overline{T'\frac{\partial^2 u'}{\partial x_j^2}})}_{R}.$$

Here a and b are two arbitrary constants. In our case we have chosen a to be 1 and b to be 0, so that the rest term only has one component instead of two. Partly due to the fact that in our case Pr lies close to one, the rest term turns out to be very small in our calculations, so we have neglected this term in our further discussion. Nevertheless, for reasons of completeness this term is also shown in the equations.

Most of the budget terms can be subdivided further into several components. Here, we will consider the contributions to the production term, which can be subdivided into production by the mean velocity gradient (G_w) and by the mean temperature gradient term (G_T); the contributions to the transport term, which can be subdivided into an advection (T_a), pressure (T_p) and diffusive part (T_d) and the contributions to the dissipation term (E), which can be divided into the separate contributions in the three directions E_x, E_y and E_z.

Other terms of which the subdivision is studied, are the pressure-strain (Φ) and the pressure transport term (T_p), where one usually distinguishes a rapid, slow, buoyant and wall part. The subdivision of the pressure terms for our flow case will be defined in the following section.

Before discussing the results of the budgets, we can first make some general arguments about the behaviour of the budgets by considering the equations that govern these budgets. We will first show that in the near wall region we always find an equilibrium between viscous transport and dissipation at (and near) the wall, both for the turbulent budgets as well as for the budget of the first unstable mode. This will be done with the knowledge that all fluctuations as well as all span-wise and vertical gradients are zero at the wall.

When we have two variables a' and b', representing a fluctuating velocity or temperature, the viscous transport term of $a'b'$ can be written as

$$\frac{\partial^2 a'b'}{\partial x_j} = a'\frac{\partial^2 b'}{\partial x_j^2} + 2\frac{\partial b'}{\partial x_j}\frac{\partial a'}{\partial x_j} + b'\frac{\partial^2 a'}{\partial x_j^2}. \tag{14}$$

At the wall a' and b' are zero, just as the vertical and span-wise gradients, and we find from Eq. (14) that

$$\left.\frac{\partial^2 a'b'}{\partial x_j}\right|_w = 2\left.\frac{\partial b'}{\partial x}\frac{\partial a'}{\partial x}\right|_w. \tag{15}$$

At the wall (denoted with subscript w) as said, the y- and z-gradients of the variances are zero and the dissipation term (E) is reduced to the x-component, which is exactly the right hand side of Eq. (15). This x-component has non-zero values at the wall for $\overline{v'v'}$, $\overline{w'w'}$, $\overline{w'T'}$ and $\overline{T'T'}$.

Next we will show that in the budgets for the instability mode the advective transport term is zero. The advective transport term is defined as

$$T_a = \frac{\partial \overline{u'a'b'}}{\partial x}, \tag{16}$$

where the overbar is defined as the integration over one wavelength in the z-direction. As we have substituted sinusoidal functions to solve this linear stability problem, u', a' and b' can be written as

$$\begin{aligned} u'(x,z) &= U(x)\sin(\alpha z + \phi_u),\\ a'(x,z) &= A(x)\sin(\alpha z + \phi_a),\\ b'(x,z) &= B(x)\sin(\alpha z + \phi_b), \end{aligned} \tag{17}$$

where α is the wavenumber of the first instability mode. Hence,

$$\overline{u'a'b'} = U(x)A(x)B(x)\int_0^{2\pi/\alpha}\sin(\alpha z + \phi_u)\sin(\alpha z + \phi_a)\sin(\alpha z + \phi_b)\mathrm{d}z' = 0. \tag{18}$$

3. The pressure terms

The pressure terms play an important role in the redistribution of the velocity variances as well as the destruction of the fluxes $\overline{u'w'}, \overline{u'T'}$ and $\overline{w'T'}$. Various physical processes contribute to the pressure term. Their contribution can be recognised individually, if we split the pressure term into its individual components. As a result, we can better understand the physics of these individual components and their contribution to the flow. For instance, in turbulence modelling it can help to reduce the number of free parameters (Dol et al., 1998). In this section we will describe this splitting procedure; the results of the splitting are shown in Section 7.

We start from Eq. (1). For the three components of the momentum equation, we differentiate with respect to x_i and then add the three equations. With aid of the continuity equation the following Poisson equation for p' is obtained:

$$\nabla^2 p' = \underbrace{-RaPr\frac{\partial T'}{\partial z}}_{B} \underbrace{-2\frac{\partial \overline{W}}{\partial x}\frac{\partial u'}{\partial z}}_{R} \underbrace{-\left(\frac{\partial u'}{\partial x}\frac{\partial u'}{\partial x} + \frac{\partial v'}{\partial y}\frac{\partial v'}{\partial y} + \frac{\partial w'}{\partial z}\frac{\partial w'}{\partial z} + 2\frac{\partial u'}{\partial y}\frac{\partial v'}{\partial x} + 2\frac{\partial u'}{\partial z}\frac{\partial w'}{\partial x} + 2\frac{\partial v'}{\partial z}\frac{\partial w'}{\partial y}\right)}_{S}. \tag{19}$$

By considering the momentum equation in the x-direction of Eq. (1) at the two walls, we arrive at the boundary conditions for this pressure equation:

$$\left.\frac{\partial p'}{\partial x}\right|_{w} = \mathrm{Pr}\left.\frac{\partial^2 u'}{\partial x^2}\right|_{w}. \tag{20}$$

As Eq. (19) is linear in p', the superposition principle is valid. We can thus solve the pressure Eq. (19) for each source term on the right hand side separately. When added together, these solutions render the complete pressure field.

By this procedure, the pressure equation is split into four different parts. We distinguish a buoyant part (p'_B), representing all contributions of the buoyant forces to the pressure term, a rapid part (p'_R), representing all contributions of the average flow, and a slow part (p'_S), representing all contributions of the velocity fluctuations. All equations are solved with homogeneous boundary conditions $\partial p'/\partial x = 0$ at the walls. The actual boundary condition (20) is solved with the equation $\nabla^2 p' = 0$. This solution accounts for the wall effect (p'_W). In Table 1 the various components of our splitting procedure have been indicated schematically. The resulting Poisson equation for each of the components is solved with the same technique as used in the main numerical code. The various pressure terms are then substituted in Eqs. (6)–(9). For instance for the pressure transport of $\overline{u'v'}$ this leads to

$$\underbrace{\frac{\partial \overline{u'p'}}{\partial x}}_{T_p} = \underbrace{\frac{\partial \overline{u'p'_B}}{\partial x}}_{T_{p_B}} + \underbrace{\frac{\partial \overline{u'p'_R}}{\partial x}}_{T_{p_R}} + \underbrace{\frac{\partial \overline{u'p'_S}}{\partial x}}_{T_{p_S}} + \underbrace{\frac{\partial \overline{u'p'_W}}{\partial x}}_{T_{p_W}}. \tag{21}$$

Table 1
Various pressure components

Pressure component	$\nabla^2 p'$	$\partial p'/\partial x\|_w$
Rapid	R, Eq. (19)	0
Slow	S, Eq. (19)	0
Buoyant	B, Eq. (19)	0
Wall	0	$\mathrm{Pr}\partial^2 u'/\partial x^2$

Following Rotta (1972), it can be proven that this method of calculating the separate pressure terms is equivalent to the theoretical explanation given in Mansour et al. (1988).

3.1. Numerical techniques

We have used a DNS technique to compute the turbulent flow properties. To apply this technique, the set of equations (1) has been formulated on a three-dimensional grid with the help of a standard finite volume method. The resulting equations are then discretized and solved with a second-order scheme. By applying this solution method on two grids. which differ approximately by a factor of 2 in each direction, we reach fourth-order accuracy of the solution through application of the Richardson extrapolation technique. By means of computation on several grids, this technique has been tested to produce indeed a fourth-order accurate solution.

As a result of the infinite extent in the vertical and spanwise direction, one can consider the flow as being homogeneous in those directions. As a consequence, we can apply our DNS in a finite, but sufficiently large vertical domain by using periodic boundary conditions. Moreover, homogeneity implies that all statistical quantities are only a function of the distance x between the two walls. The grid-size varies along the x-direction. From the wall towards the centre each grid volume is increased by a constant factor in such a way that the smallest grid-size near the wall is three times smaller than the largest grid-size in the centre of the channel. The grid in the other two coordinate directions has been chosen to be uniform. In Table 2 we have summarised all important computational details.

4. Average profiles

To give an impression of the flow characteristics and our numerical results, we show in Fig. 3 the average velocity and temperature profiles for the four Rayleigh numbers that we have computed. We have also plotted the laminar velocity and temperature profiles Eq. (4) in these figures. Furthermore, some of the experimental data (Betts and Bokhari, 1996), have been also plotted in the same figures. These values have been measured in a tall enclosure at $\mathrm{Ra} = 8.3 \times 10^5$.

The figures can be subdivided roughly into two regions. First, a region near the wall; here, viscosity is important, because the turbulent stresses and fluxes are small compared to these stresses and fluxes in the centre region. Second, the centre region in between the two velocity maxima; here, the turbulent fluxes are high compared to the viscous fluxes.

As Ra increases, also the average velocity increases and also the buoyant forces. Together with the increasing average velocity the turbulence level increases as well. The increasing turbulence level induces an increase in the heat exchange in the centre region. As a result, the average temperature gradient

Table 2
Computational details

Computational domain	$L_z \times L_y \times L_x = 12.0 \times 6.0 \times 1.0$
Number of grid points (coarse)	$N_z \times N_y \times N_x = 180 \times 90 \times 48$
Resolution in x-direction	$\Delta x_{\min} = 0.000975\ h$ at the wall
	$\Delta x_{\max} = 0.00292\ h$ at the centre
Number of grid points (fine)	$N_z \times N_y \times N_x = 432 \times 216 \times 96$
Resolution of x-direction	$\Delta x_{\min} = 0.000439\ h$ at the wall
	$\Delta x_{\max} = 0.00131\ h$ at the centre
Rayleigh numbers computed	$\mathrm{Ra} = 5.4 \times 10^5$, 8.227×10^5,
	2.0×10^6, 5.0×10^6

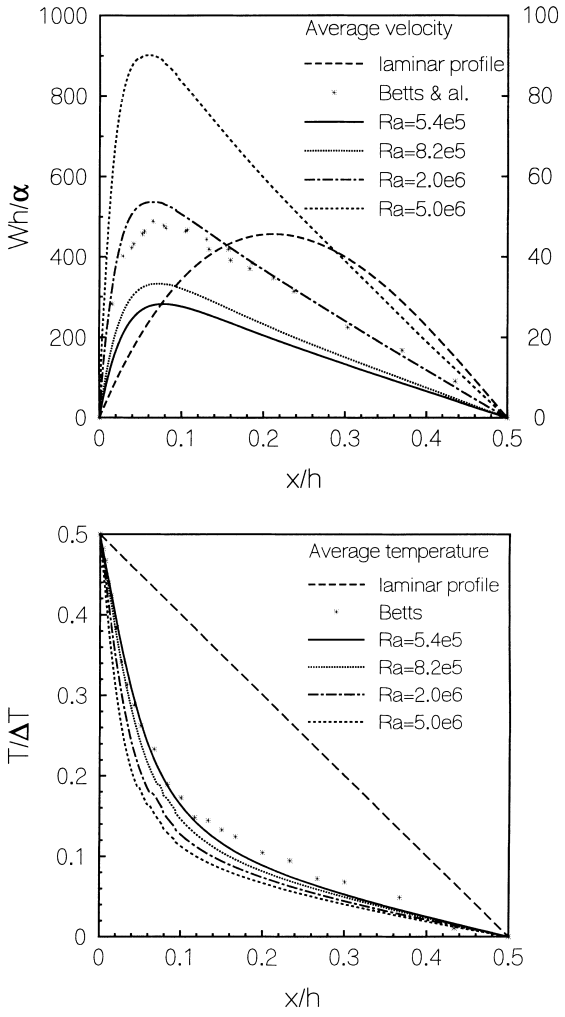

Fig. 3. Mean vertical velocity and temperature profile for the four Rayleigh numbers that have been computed together with the experimental values (left y-axis) and the laminar profiles. The laminar velocity profile is given at $\mathrm{Ra}_{cr}(=5699)$ and its scale is on the right y-axis.

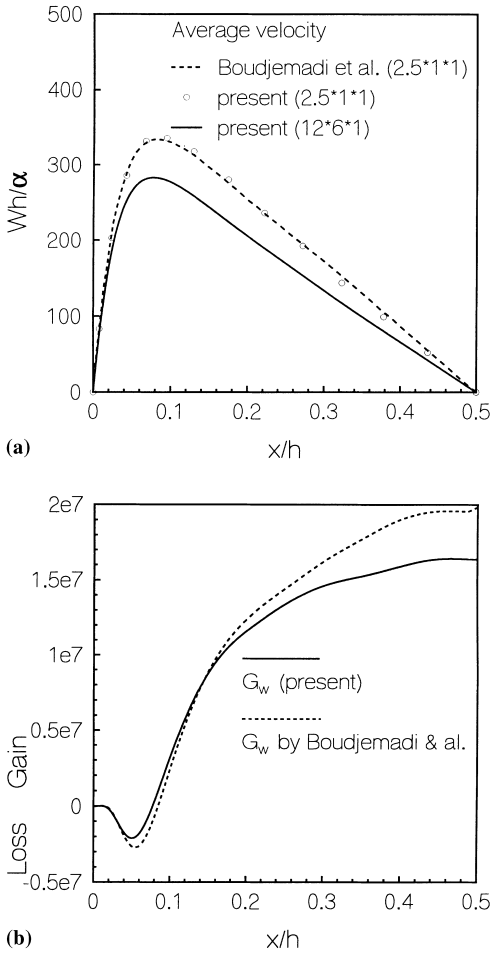

Fig. 4. (a) Average velocities at $\mathrm{Ra} = 5.4 \times 10^5$ for different domain sizes. (b) Shear production term for $\overline{w'w'}$.

in the centre decreases, while the average temperature gradient near the wall increases. Furthermore, the velocity maximum moves towards the wall with increasing Ra.

The measured velocities and temperature are found to be higher than the numerical data at about the same Ra. The discrepancy between the measurements and the numerical calculations may have been caused by the lower turbulence level in the measurements. Due to the fact that the enclosure is finite, the turbulence may not have been fully developed, thus allowing a higher velocity and temperature gradient in the centre region.

In Fig. 4(a), we have plotted the average velocity profile obtained by Boudjemadi et al. (1997) for $\mathrm{Ra} = 5.4 \times 10^5$. For their numerical calculations they used a domain size of $L_z \times L_y \times L_x = 2.5 \times 1.0 \times 1.0$. For comparison we have plotted our results for a domain size equal to Boudjemadi et al. (1997), as well as our results for the large computational domain given in Table 2. Both our results and the results of Boudjemadi et al. (1997) agree very well as far as the small computational domain is concerned. However, for the large computational domain our average velocity profile is significantly lower. As we were able to reproduce the results of Boudjemadi et al. (1997) when using a similar domain, we feel allowed to draw the conclusion that a domain size when it is chosen too small, is not able to represent the infinite domain in an adequate way. This conclusion is confirmed by the fact that Komminaho et al. (1996) reported large structures in the closely related plane Couette flow.

In another study, we will consider the size of coherent structures in this flow; in the next paragraph we will only give a short explanation for the fact that a small domain size can lead to higher average velocities.

Let us consider the two-point-correlation function (C_2) in the spanwise y-direction. This correlation is defined as

$$C_2(y) = \frac{\overline{\Psi(y_0)\Psi(y_0+y)}}{\overline{\Psi(y_0)^2}}, \tag{22}$$

with Ψ an arbitrary variable.

In Fig. 5(a) we show this autocorrelation function for the centre region, i.e. $x = 0.5$ (where the turbulence intensity is highest). We can see that at a separation of about $1h$ the autocorrelation of the vertical velocity and temperature reaches a minimum value, i.e. the turbulent part of the vertical velocity at $y_0 + h$ is opposite on average, compared to the vertical velocity at y_0. Therefore, we conclude that the size of the main structures in the y-direction measures about $2h$, which is close to the size of the structures in the vertical direction. This size does not fit into the calculation domain of Boudjemadi et al. (1997). As a result, the turbulence is damped and an 18% higher velocity gradient can be established. The temperature field is

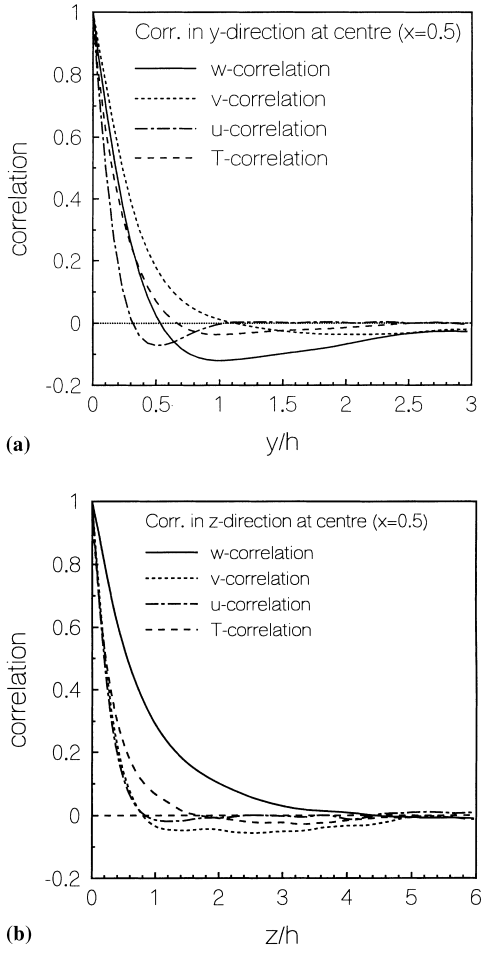

Fig. 5. Two-point-correlations for the velocities and temperature in the centre regions (a) in the spanwise direction; (b) in the vertical direction.

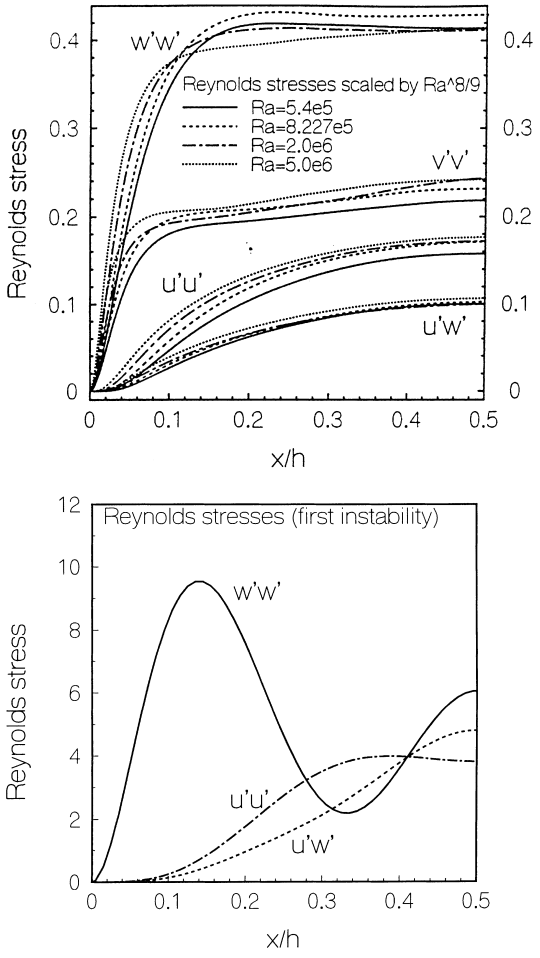

Fig. 6. Non-zero components of the Reynolds-stress tensor scaled by $Ra^{\frac{8}{9}}$ (top) and the same components obtained from the first unstable mode (bottom).

only slightly affected. The resulting higher velocity gradient partly obscures the decreased turbulence level, because the turbulence production given in Fig. 4 increases with increasing velocity gradient according to Eq. (9). This results, mainly in the centre region, in a higher turbulence production.

5. Stresses, fluxes and variances

In this section we will make a comparison between the turbulent stresses and fluxes that we have computed with aid of DNS and the stresses and fluxes that we have computed from the first instability mode. We should note that the amplitude of the first linear instability is a free parameter, i.e. independent of the laminar flow profile. Here we have normalised all stresses and budgets in such a way that the maximum for the streamfunction of the first instability mode is equal to 1.

The non-zero components of the Reynolds-stress tensor are shown in Fig. 6. For the values obtained at the four Rayleigh numbers, we have used the scaling that we have introduced at the end of Section 2.1. We find that the turbulent velocity fluctuations can be as large or even larger than the mean velocity. Therefore, instantaneous velocities can occur which have a direction opposite to the mean flow, even in the region around the velocity maximum. Also the temperature fluctuations can reach a high level. A fluctuation with a value that is 25% of the mean temperature difference between the two walls is no exception.

In Fig. 6 (bottom) we also show the stresses obtained from the first instability mode. We can see that in the near wall region the behaviour of the stresses looks similar. At $x \approx 0.33$, a large dip can be found for $\overline{w'w'}$. In this region w' is re-converted into u', as may be observed from the streamfunction patterns in Chait and Korpela (1989) or Versteegh (1998). This behaviour depends also on the Prandtl number. For low Pr, i.e. when the main instability factor is shear, this dip in the centre region is less pronounced.

The turbulent profiles for the temperature fluxes (see Fig. 2(a)) are completely different from those of the first instability. The $\overline{u'T'}$-flux for the first instability shows a very small but negative minimum which is not apparent in the turbulent budget. Here the linear stability analysis shows its drawback when it is used for comparison with a turbulent flow. Together with the assumption that the average temperature gradient remains constant, the horizontal velocity fluctuations can act as a local heat source, according to the advection term $u'\partial\overline{T}/\partial x$ in the temperature equation of (5). In other words, local heat production for the secondary flow structure does not effect in a heat loss for the average flow. As a result, an average negative horizontal heat flux is possible from the local heat source towards the wall in linear stability analysis. This cannot be the case when non-linear effects are considered. After all, before heat can be transported towards the wall, first it has to be transported from the wall towards that location.

The behaviour of vertical heat flux $\overline{w'T'}$, which is related to the buoyant energy production, is also different for the turbulent flow than for the first instability. From linear stability analysis we found that the secondary flow is mainly driven by shear energy production in the centre region (Versteegh, 1998). In the near wall region the secondary flow opposes the buoyant force on average. Here, the kinetic energy is partly destroyed by buoyancy. As a result, the $\overline{w'T'}$-flux for the first instability shows a pronounced negative minimum in the near wall region. In the turbulent case the average temperature gradient is affected and a large average temperature gradient in the near wall region is found, whereas in the centre region the temperature gradient is small. The large temperature gradient near the wall results in large temperature fluctuations and combined with the high Rayleigh number, this results in a large buoyant force that cannot be opposed by the local flow structure. As a result the vertical heat flux and buoyant energy production is positive (and large) in the near wall region.

6. Budgets

The budgets of the Reynolds-stress components, temperature fluxes and temperature variances for turbulent flow are shown in Figs. 7–13. For each component (except $\overline{v'v'}$) the budget has also been computed for the first instability mode. The results of the turbulent budgets and the budgets of the first instability mode are shown together. A comparison leads us to the conclusion that many characteristics of the presented stress budgets are qualitatively similar for the turbulent flow and the first instability mode. However, the budgets for the temperature fluxes and temperature variances are different. This discrepancy in the temperature budgets becomes also clear in some buoyant budget terms in the Reynolds stresses. The discrepancy can be explained by considering Eqs. (10)–(12). In the previous section we concluded that the average temperature gradient and the horizontal temperature flux in the turbulent case are completely different from those of the linear instability. As a result the production terms for the temperature fluxes and temperature variances are completely different, and if the production terms are different the entire budget will be different. As an example, we regard the production term for the $\overline{T'T'}$-budget given in Fig. 7. This term is equal to $\overline{u'T'}\partial\overline{T}/\partial x$, according to Eq. (12). For the first instability the average temperature gradient is constant over the entire flow geometry; therefore the maximum in the $\overline{T'T'}$-variances can be found where the horizontal velocity fluctuations are largest, i.e. in the centre. For the turbulent case, however, the average temperature gradient in the centre is very small. Here the maximum is found near the wall, where both the average temperature gradient as well as the velocity fluctuations are considerably large. While the temperature gradients in the near wall region become larger with increasing Ra, the gradients in the centre region become smaller; the maximum in the produc-

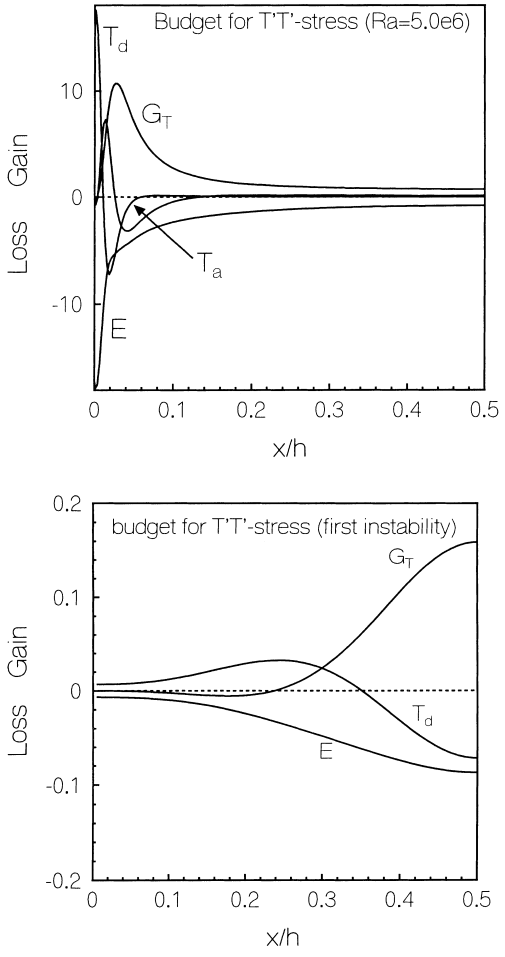

Fig. 7. The turbulent $\overline{T'T'}$-budget scaled by $Ra^{\frac{1}{5}}$ (top) and the $\overline{T'T'}$-budget of the first instable mode (bottom).

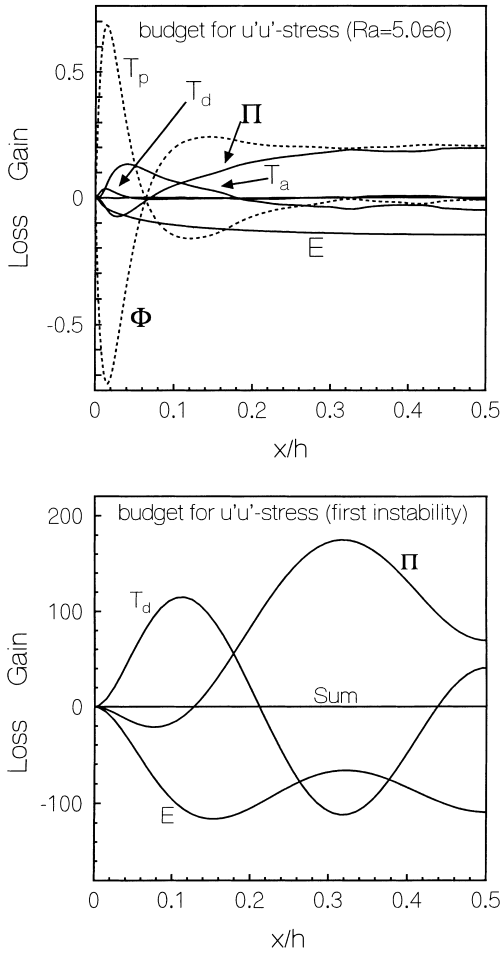

Fig. 8. The turbulent $\overline{u'u'}$-budget scaled by $Ra^{\frac{8}{9}}$ (top) and the $\overline{u'u'}$-budget of the first unstable mode (bottom).

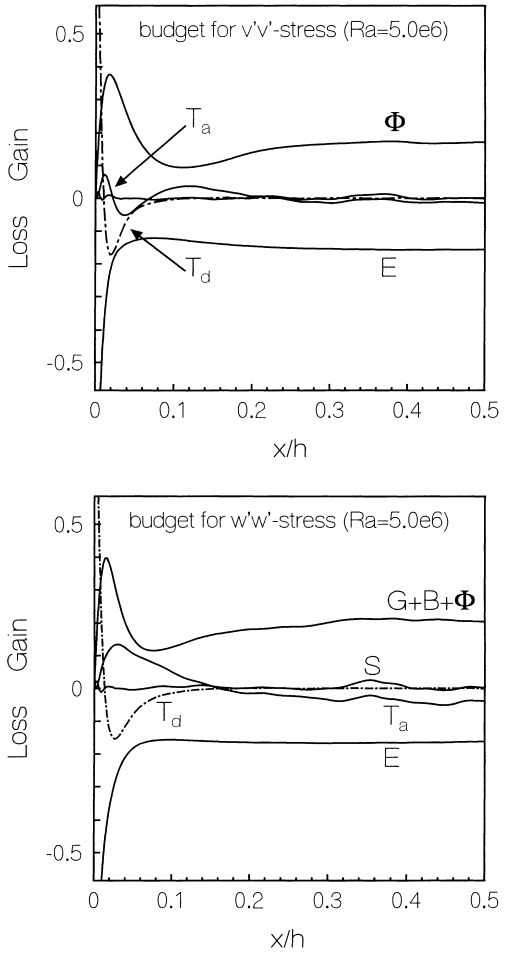

Fig. 9. The turbulent $\overline{v'v'}$-budget scaled by $Ra^{\frac{8}{9}}$ (top) and the $\overline{w'w'}$-budget with combined terms (bottom).

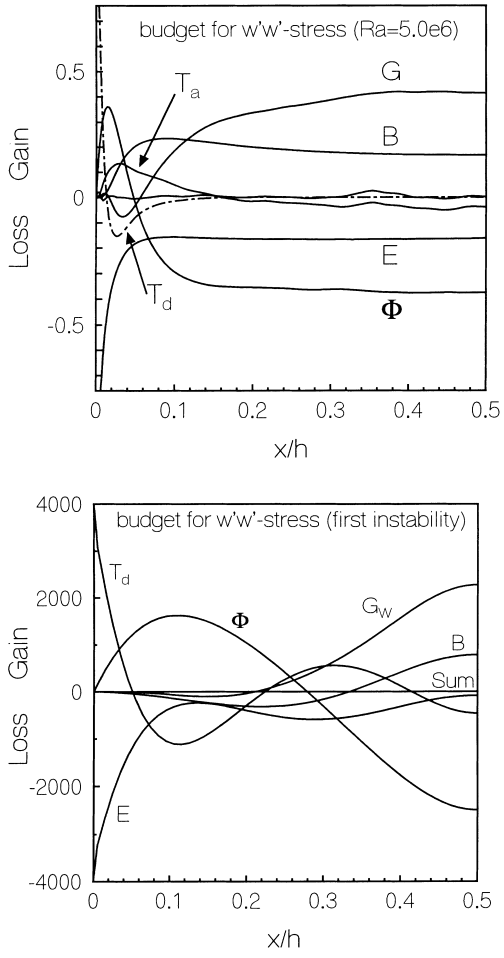

Fig. 10. The turbulent $\overline{w'w'}$-budget scaled by $Ra^{\frac{8}{9}}$ (top) and the $\overline{w'w'}$-budget of the first unstable mode (bottom).

tion term in the near wall region increases relative to the production in the centre region.

Next, the budgets are considered in somewhat more detail. We will only show results for the highest value of the Rayleigh number, i.e. $Ra = 5.0 \times 10^6$, since most of the features in the budget remain similar within the range of Ra what we have studied (Versteegh, 1998).

We will first consider the budgets of the normal stresses. When summed, the budget terms G, B, T, Φ end E in Eqs. (7)–(9) describe the production buoyancy, transport, redistribution and dissipation of the turbulent kinetic energy. Note again that in the turbulent kinetic energy equation these terms appear multiplied with a factor 1/2.

Both production terms of turbulent kinetic energy (G and B) appear only in the $\overline{w'w'}$-budget, i.e. shear and buoyancy directly produce vertical velocity fluctuations. The energy in the vertical direction is then converted into $\overline{u'u'}$ and $\overline{v'v'}$ by means of the pressure–strain term (Φ). This term links the budgets of the three variance components, because it follows from the continuity equation that the sum of the Φ-terms over the three coordinate directions is zero. One usually assumes that this interaction between Φ-terms in the three directions is in balance when the turbulent energy is the same in all directions, i.e. the turbulent flow isotropic. Therefore, the Φ_{ii}-term is sometimes called the return-to-isotropy term, based on the hypothesis formulated by Rotta (1951). A return-to-isotropy behaviour of the Φ_{ii}-term is found in the centre region between the two walls. In the near wall region anisotropic effects come into play. Namely, due to the wall influence, the Φ_{ii}-term acts in such a way that motion perpendicular to the wall is transformed into motion along the wall, i.e. anisotropy is increased. Such a behaviour is called "splatting" (Chapman and Kuhn, 1986) in turbulence modelling, and can be confirmed from the dip in $\Phi_{u'u'}$ and the peak in $\Phi_{v'v'}$ and $\Phi_{w'w'}$ in the near wall region.

In Fig. 6(top), we can see that in the centre region, relative to the $\overline{w'w'}$-stress, the $\overline{u'u'}$- and $\overline{v'v'}$-stress show an increase with increasing Ra. This implies that with increasing Ra the return-to-isotropy-terms increase, compared to the turbulence production terms that only create turbulent motion in the vertical direction. However, in our opinion, even for very high Ra, the turbulence will not become isotropic because of the following reason. The return-to-isotropy-terms decrease the more isotropy is reached, whereas the anisotropic production terms will remain producing turbulent energy in the vertical direction. Because the ratios of $\overline{u'u'}$, $\overline{v'v'}$ and $\overline{w'w'}$ already seem to converge in our calculations, we think that the relation $\overline{w'w'}$: $\overline{v'v'}$: $\overline{u'u'}$ for $Ra = 5.0 \times 10^6$ lies already close to its limit value. In Table 3 these values for $Ra = 5.0 \times 10^6$ are given.

For the $\overline{u'u'}$-budget and the flux budgets for $\overline{u'w'}$, $\overline{u'T'}$ and $\overline{w'T'}$, we find that in the near wall region primarily T_p and Φ are quite large and almost in equilibrium. On the other hand, T_p is relatively small in the centre region. Let us therefore

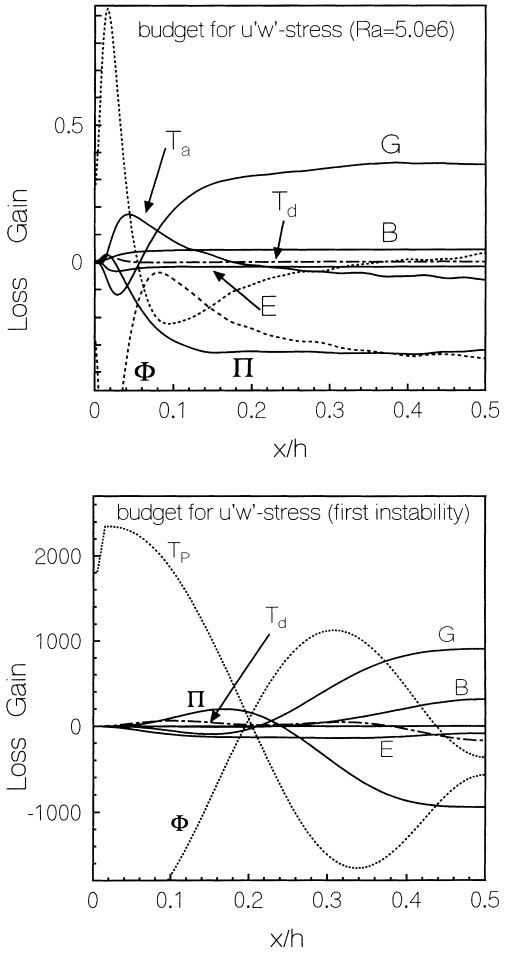

Fig. 11. The turbulent $\overline{u'w'}$-budget scaled by $\mathrm{Ra}^{\frac{8}{9}}$ (top) and the $\overline{u'w'}$-budget for the first unstable mode (bottom).

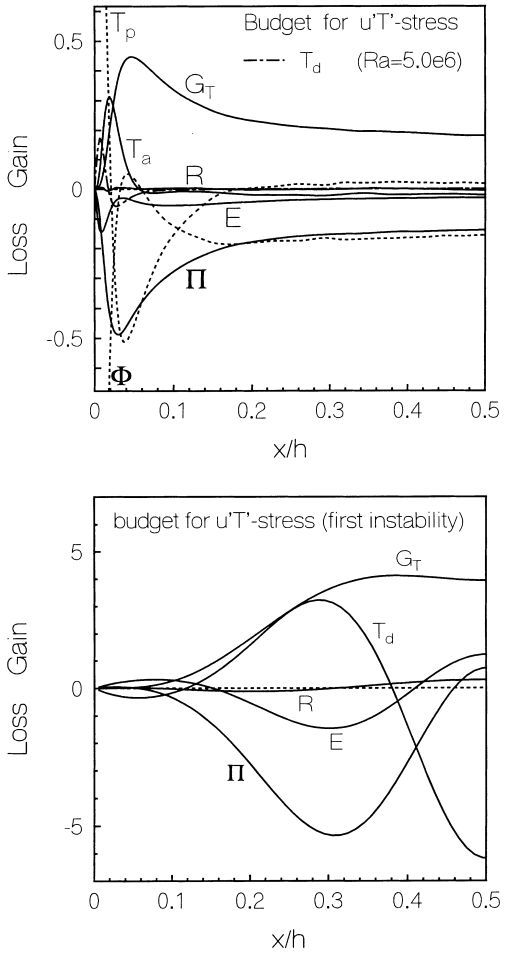

Fig. 12. The turbulent $\overline{u'T'}$-budget scaled by $\mathrm{Ra}^{\frac{7}{9}}$ (top) and the $\overline{u'T'}$-budget of the first instability (bottom).

denote the combination $T_p + \Phi$ as Π. The results shown in the Figs. 8, 11–13 suggest that Π behaves in a more continuous way and that the values of Π near the wall are for instance quite small. Therefore, it seems that the behaviour of Π might be more easily modelled, than the separation of Π into T_p and Φ, which is usually done in turbulence modelling. This is especially attractive for the flux budgets of $\overline{u'w'}$, $\overline{u'T'}$ and $\overline{w'T'}$, where the interpretation of interactions between the Φ-terms in the three coordinate directions, as discussed above, is not useful. For a modeller's point of view the reader is referred to Dol et al. (1997b) and Dol et al. (1998).

Because of their large magnitude, the Φ- and T_p term are not shown in the $\overline{u'u'}$-budget of the first unstable mode in Fig. 8 (bottom), but their behaviour is similar to that of the turbulent $\overline{u'u'}$-budget. Also for the other terms in the $\overline{u'u'}$-budget, a similar behaviour as found in the turbulent budget can be observed in the budget of the first unstable mode.

The dissipation terms for the fluxes $\overline{u'w'}$, $\overline{u'T'}$ and $\overline{w'T'}$ are small. In these budgets the role of destruction is for a large part taken over by the Φ- or Π-term. This is in contrast with the kinetic energy budgets, where all terms involving pressure only have a redistributive character; the loss in the $\overline{w'w'}$-budget is exactly equal to the production in the $\overline{u'u'}$- and $\overline{v'v'}$-budget and the pressure transport term for the $\overline{u'u'}$-budget is zero when integrated over the distance between the two walls.

For reasons of symmetry it can be proven that for isotropic turbulence the dissipation term for the fluxes $\overline{u'w'}$, $\overline{u'T'}$ are $\overline{w'T'}$ is zero. The relative magnitude of the dissipation term can therefore be interpreted as the level of anisotropy. For $\mathrm{Ra} = 5.0 \times 10^6$, the pressure destruction for the fluxes in our flow problem is much larger than the regular viscous dissipation. In the worst case, namely $\overline{u'T'}$, in the centre region about 75% is dissipated by pressure, the rest by the dissipation term. For the other two fluxes $\overline{u'w'}$ and $\overline{w'T'}$, the relative contribution by the pressure dissipation is even higher. From this we can conclude that the flow in the centre region already reached a high level of isotropy. With increasing Ra this isotropy level has a tendency to increase.

Near the walls large gradients and strong dissipation of the variances and fluxes occur, because all variances and fluxes have to be zero at the wall. These large gradients induce a large viscous transport towards the wall that balances the dissipation. As a result, we find that for $\overline{v'v'}$, $\overline{w'w'}$, $\overline{w'T'}$ and $\overline{T'T'}$, $T_d = E$ is a good approximation. In fact, such a balance is consistent with the condition on the wall where an equality between T_d and E must be satisfied exactly. For $\overline{u'u'}$, $\overline{u'w'}$ and $\overline{u'T'}$ a similar equilibrium should be valid. It may however be somewhat obscured for the following reasons. First, the dissipation and transport terms for these components are exactly zero at the wall. Secondly, T_p and Φ have been found to be large near the walls. However, the combination of these terms in Π results in a much smaller value near the wall so that T_d and E may again become dominant.

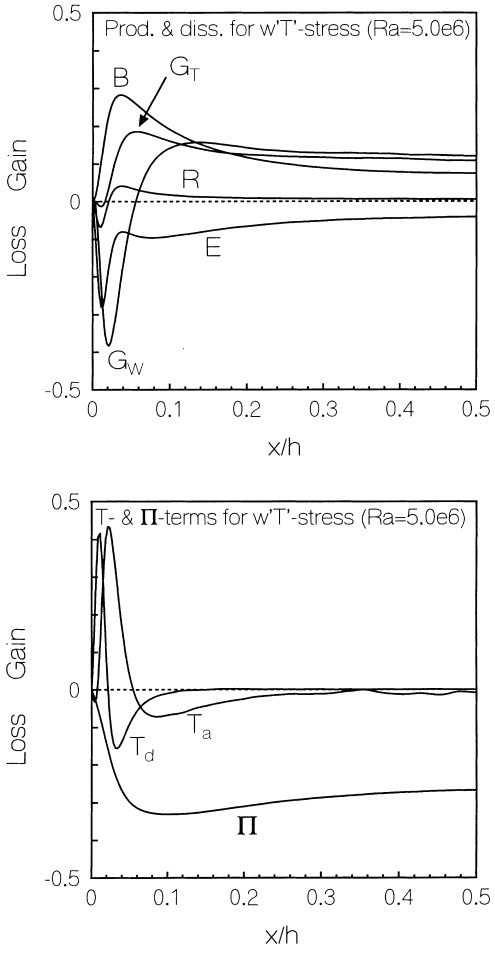

Fig. 13. The turbulent $\overline{w'T'}$-budget scaled by $Ra^{\frac{7}{9}}$.

Transport terms are generally only large in regions where the second derivative of the stress term considered is large. In the centre region the second derivative for $\overline{v'v'}$, $\overline{w'w'}$, $\overline{w'T'}$ and $\overline{T'T'}$ is small, therefore their transport terms are small and a balance, *pressure or production* term = *destruction or dissipation term*, is a good first approximation. Only for $\overline{u'u'}$ and $\overline{u'w'}$ this is not completely true and we find that the transport term in this case is about 30% of the production for $\overline{u'u'}$ and about 15% for $\overline{u'w'}$.

As shown in Eq. (16) T_a is zero for the budgets of the first instability mode. Also in the turbulent budgets T_a is relatively unimportant except in the region around the velocity maximum, where T_a cannot be neglected. Here, the rapid increase of the stresses and fluxes in the near wall region is replaced by a slower increase towards their maximum in the centre. The large second derivatives of the stresses caused by this effect, enhance advective transport.

When the first instability budget is considered, also an equilibrium between the viscous terms near the wall is observed.

Table 3
Ratios of the stress components

Relative stress term	Ratio
$\overline{u'u'}/\overline{w'w'}$	0.43
$\overline{v'v'}/\overline{w'w'}$	0.59
$\overline{u'w'}/\overline{w'w'}$	0.25

Contrary to the $\overline{w'w'}$-stress, which is rather constant in the centre region, the $\overline{u'u'}$- and $\overline{u'w'}$-stress show a decrease towards the wall. This is due to the solid wall which damps perpendicular motion much more strongly than motion along the walls. As a result, near the velocity maximum the second derivative of $\overline{u'u'}$ and $\overline{u'w'}$ are zero. This inflection point causes a constant $\overline{u'u'}$- and $\overline{u'w'}$-transport from the centre region and the wall region towards the region of the velocity maximum. Therefore, in this region an equilibrium between transport and dissipation is established.

Both in the $\overline{u'w'}$- and in the $\overline{w'w'}$-budget, the shear production is negative in the region between the wall and the velocity maximum. This property is also present in the budgets of the first instability modes for these terms, although G_W is only slightly negative in the first instability budget. Such negative production has also been observed in the buoyant flow along a single vertical plate (Henkes, 1990). This negative shear production has not been found in experiments of Tsuji and Nagano (1988), but Nagano et al. (1989) claimed that, with increasing compressibility of the fluid, this negative production may vanish. For further details on this property we refer to Versteegh (1998).

Also for the $\overline{w'T'}$-budget the shear production is negative between the wall and the velocity maximum, however this can be explained rather easily. Due to the positive average velocity gradient ($\partial\overline{W}/\partial x > 0$) between the wall and the velocity maximum, whereas the turbulent temperature flux $\overline{u'T'}$ is positive over the entire domain, G_W is negative between the wall and the velocity maximum. In the centre region the gradient production is positive; furthermore, the three production terms are almost equal in size in this region. With increasing Ra the buoyant term becomes less important than the other two terms.

The span-wise and vertical variance budgets, i.e. the $\overline{v'v'}$ and $\overline{w'w'}$ terms, show many similarities. Let us consider the combination of the two production terms and the pressure–strain term for the $\overline{w'w'}$-budget into a single term. The result is shown in Fig. 9 (bottom). The profiles of Fig. 9 (top) and (bottom) are almost identical. This resemblance appears also in the $\overline{v'v'}$- and $\overline{w'w'}$-profiles that exhibit many similarities, except for their magnitude. The exception in both budgets is the advective transport term. This term that can almost be neglected for the $\overline{v'v'}$-budget can certainly not be neglected for the $\overline{w'w'}$-budget. A possible reason for this is the fact that around the velocity maximum there is a considerable amount of buoyant energy production, that amplifies the inflection point in the $\overline{w'w'}$-stress profile.

For a final point we return to a comparison between the turbulent budgets and the same budgets computed from the first instability modes. We can see that the curves resulting from the budgets of the first instability mode are more stretched out in the near-wall region than for the turbulent budgets. In other words, the centre region for the first instability mode budgets is much smaller than for the turbulent budgets, for which the x-dependence is only small in the centre region. This is caused by the fact that the velocity maximum for the first instability mode lies much further from the wall than in the turbulent case.

7. Separate components of the dissipation and pressure terms

In the following subsections, we will give a short overview of the separate components that form the dissipation and pressure terms. We will discuss their behaviour and its implications. For more detailed information, we will refer to our data base, which contains all separate terms.

7.1. Dissipation

In Figs. 14–16 some examples of the splitting of dissipation in its components are shown.

Due to the fact that the gradients in the spanwise and vertical direction are zero at the wall, E_y and E_z are zero at the wall for all budgets. The damping effect of the wall creates high gradients of the fluxes and stresses in x-direction in the near wall region. As a result, near or at the wall E_x reaches a maximum for all budgets and dominates the dissipation term. For $\overline{v'v'}$, $\overline{w'w'}$ and $\overline{T'T'}$, the maximum in E_x lies at the wall. For $\overline{w'T'}$, the maximum of the dissipation lies somewhat remote from the wall, but the value of the wall remains non-zero. Due to continuity, $\partial u'/\partial x$ is zero at the wall, therefore the x-dissipation terms of $\overline{u'u'}$, $\overline{u'w'}$ and $\overline{u't'}$ must be zero at the wall. For these budgets the maximum in E_x also lies somewhat remote from the wall.

In the paragraph above we have given several reasons for the fact that the dissipation terms are anisotropic in the near wall region. In the free turbulent regime in the centre region, one would expect a much higher degree of isotropy in the dissipation terms. However, this is only true for the $\overline{T'T'}$-dissipation, for the other budgets this is not the case. Part of the anisotropy can be explained by the fact that the continuity constraint tends to suppress fluctuations of the kind $\partial u_i'/\partial x_i$. As a result, in the centre region (where the wall effects are diminished) E_i of all stresses and fluxes with a component u_i' is small compared to the other component(s). The fact that E_y for $\overline{u'u'}$ and $\overline{u'T'}$ is large in the centre region can probably be explained by considering Fig. 4 which shows the two-point correlations for different variables in both the y- and z-direction in the centre. Especially the correlation graph for u' in the y-direction shows a negative minimum at a shorter separa-

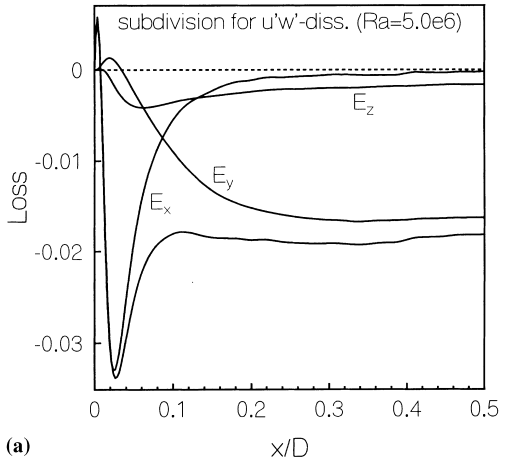

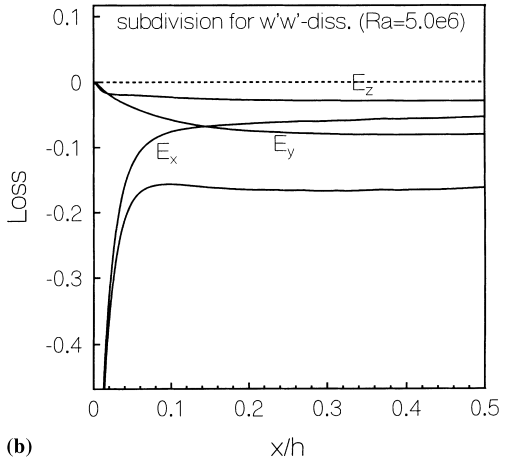

Fig. 14. (a) Subdivision of the dissipation terms for $\overline{u'w'}$. (b) Subdivision of the dissipation-terms for $\overline{w'w'}$.

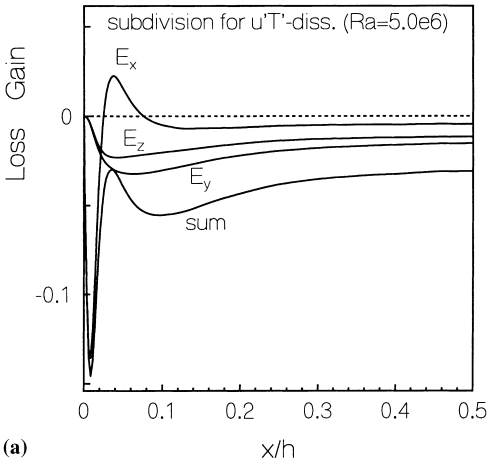

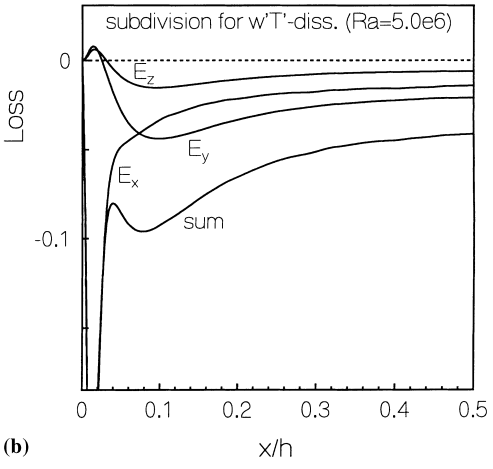

Fig. 15. (a) Subdivision of the dissipation terms for $\overline{u'T'}$. (b) Subdivision of the dissipation terms for $\overline{w'T'}$.

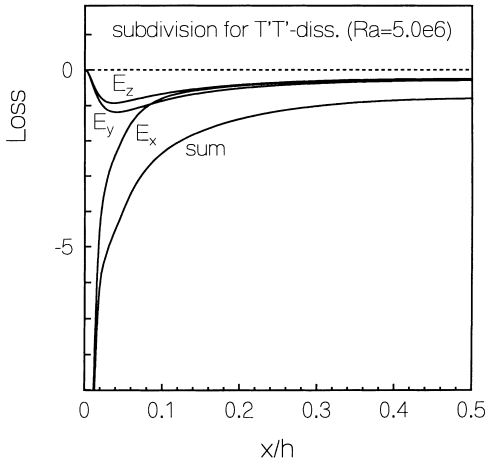

Fig. 16. Subdivision of the dissipation terms for $\overline{T'T'}$.

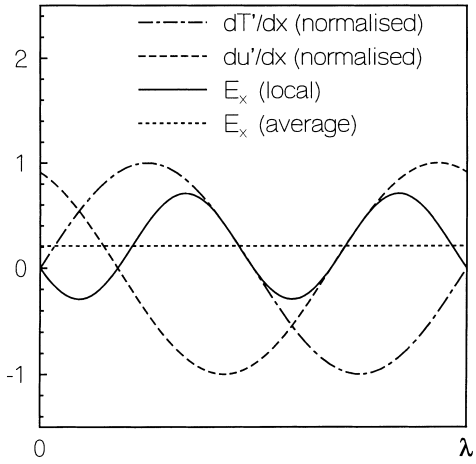

Fig. 17. Single Fourier component of $\partial u'/\partial x$ and $\partial T'/\partial x$.

tion than the other variables. Furthermore, the same minimum lies at a shorter separation than in the z-direction. It indicates small structures for u' in the y-direction. As a result, the gradients in the y-direction will be higher than in the z-direction.

For the flux budgets (both momentum and temperature) single components of the dissipation terms can become positive, even when the considered flux itself is positive. Besides some small positive regions in the dissipation for $\overline{u'w'}$ and $\overline{w'T'}$, this feature is especially significant for E_x of $\overline{u'T'}$. The examples show that the dissipation term of a cross correlation term not necessarily needs to have a dissipative character. In order to explain this phenomenon, we show an arbitrary normalised Fourier component of $\partial T'/\partial x$ and $\partial u'/\partial x$ at $x = 0.06$ (the maximum of E_x for $\overline{u'T'}$ (Fig. 17)). We can see that the waves are out of phase and as a result, the average multiplication (dissipation term) becomes positive.

7.2. Φ-terms

From Eqs. (6) to (12), we can see that the pressure transport terms are only prominent in budgets of the u'-related stresses and fluxes. In the centre region these terms are small compared to the Φ-terms, whereas in the near wall region the terms are almost exactly opposite to the Φ-terms. We will therefore pay no further attention to the pressure transport terms.

The subdivision of the Φ-terms are shown in Figs. 18–20. In the centre region, where the turbulent kinetic energy is produced, the negative Φ-term for $\overline{w'w'}$ is dominated by the slow part and a somewhat smaller rapid part. The slow part is responsible for energy transport towards the $\overline{u'u'}$-component, while the buoyant and rapid part almost entirely is transported towards the $\overline{v'v'}$- component. We can conclude that the turbulent energy which is produced by buoyancy and shear, first produces a two-dimensional structure in vertical and spanwise direction, whose energy is only indirectly transported towards $\overline{u'u'}$.

In the near wall region about half of the total energy is about equally re-converted from $\overline{u'u'}$ into $\overline{v'v'}$ and $\overline{w'w'}$ by the slow term. The other half is spread over the other components (W, R and B), whereas the wall term W appears to be the largest of the three.

Contrary to the kinetic energy budgets, the Φ-term for $\overline{u'w'}$, which is dissipative for this budget, is dominated by the rapid part in the near wall region. In the centre region the pressure term is, as in the $\overline{u'u'}$-stress, dominated by the slow part, although the rapid part cannot be neglected.

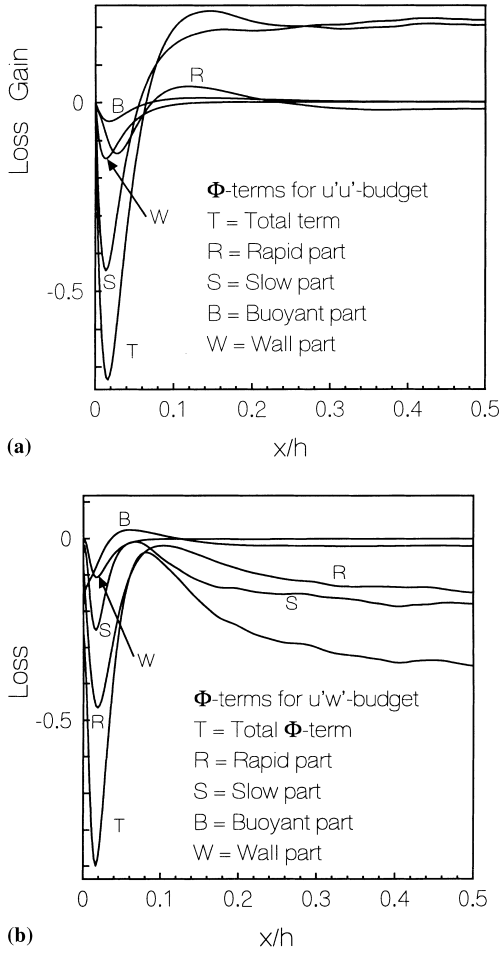

Fig. 18. (a) Subdivision of the Φ-terms for $\overline{u'u'}$. (b) Subdivision of the Φ-terms for $\overline{u'w'}$.

In the $\overline{u'T'}$-budget, only the slow pressure term (Π_s) is important, apart from a small contribution of R and W around the velocity maximum. For $\overline{w'T'}$ the slow term is also the main component but the other components cannot be neglected. Contrary to the other stresses, for $\overline{w'T'}$ the pressure terms show a gradual increase and no large peaks near the wall can be seen. The negative rapid term near the wall only appears for larger Ra and its magnitude increases with Ra.

8. Conclusions

Natural convection flow in an infinite, differentially heated, vertical channel has been studied with aid of DNS. By means of Richardson extrapolation, by considering the influence of domain size and by means of long time integration, the results presented here for turbulent flow are statistically stationary and have been calculated up to a high degree of accuracy. As we have only presented a summary of all calculated variables, we have set up a database in order to make all data available in full detail. This database can be obtained from the authors.

The main emphasis of the discussion has been put on the results for the budgets of the non-zero Reynolds-stress components, temperature fluxes and temperature variances. In accordance with Boudjemadi et al. (1997), one of our important findings is that in the near-wall region the shear production of turbulence is negative.

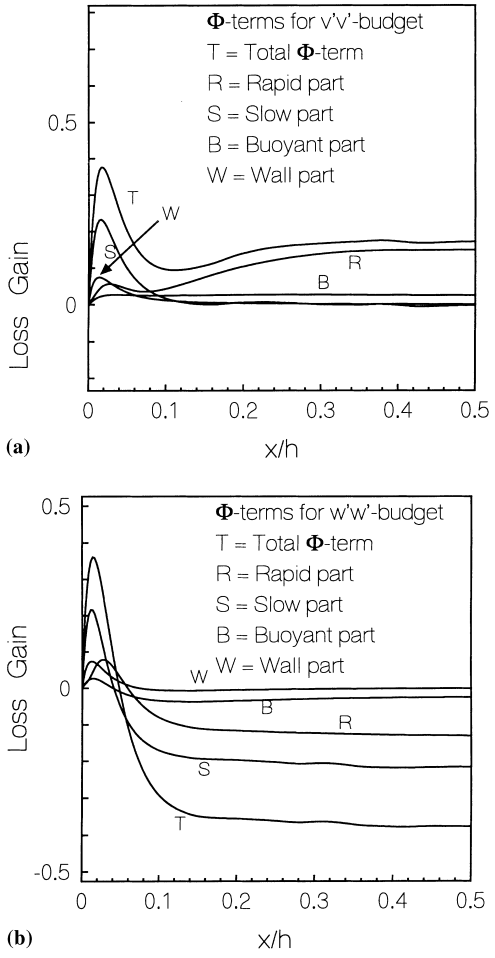

Fig. 19. (a) Subdivision of the Φ-terms for $\overline{v'v'}$. (b) Subdivision of the Φ-terms for $\overline{w'w'}$.

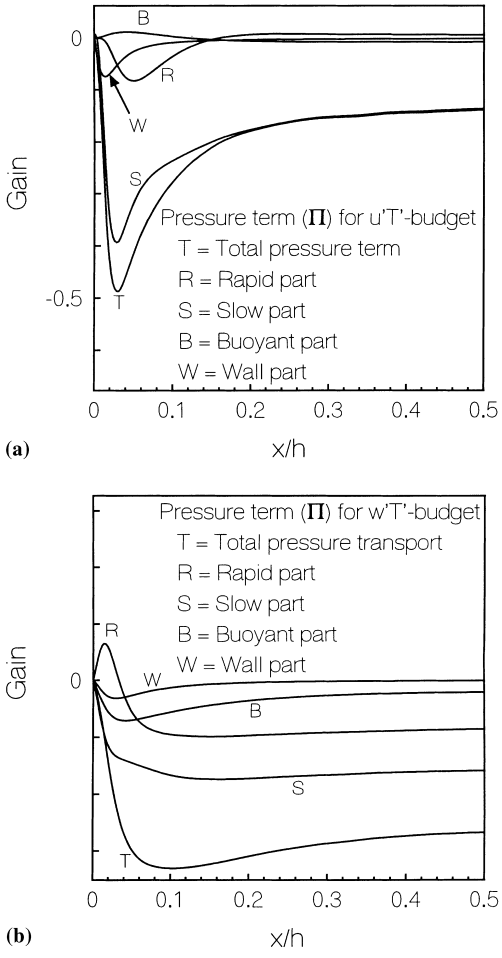

Fig. 20. (a) Subdivision of the Φ-terms for $\overline{u'T'}$. (b) Subdivision of the Φ-terms for $\overline{w'T'}$.

Separation of the original pressure term into pressure transport and a Φ-term is difficult to model. In the near wall region the terms are very large and almost exactly opposite, whereas in the centre region the pressure transport is small compared to Φ. Therefore, the Π-terms given in this paper behave in a more continuous way near the wall.

The slow part of the pressure terms is dominant over the rapid, buoyant and wall part in the near wall region. This is also the case in the centre region, except for $\overline{v'v'}$.

The turbulent budgets show that we can divide the flow into a near wall region where diffusive transport balances dissipation and a centre region where (pressure) production balances (pressure) dissipation. Only in the region near the velocity maximum does advective transport become important.

The turbulent budgets have been compared with the budgets computed from the first linear instability mode. Compared to these budgets, which show a large x-dependence in the centre region, the turbulent budgets hardly show any change in the centre region. In general, we can state that in the centre region the profiles tend to become independent of x compared to the instability budgets. Nevertheless, the turbulent stress budgets are similar to those of the first instability in many details. This leads us to the conclusion that the turbulence still contains characteristics resembling the perturbation velocity field of the first linear instability. Moreover, these patterns carry a substantial part of the energy.

For the budgets of the temperature fluxes and temperature variances comparison with the first instabilities are poor. Partly, the change in average temperature gradient can be held responsible for this, and partly, the linear stability approach. Finally, for the turbulent case, the large temperature fluctuations near the velocity maximum combined with the high Rayleigh number induce forces that destroy the original flow pattern.

References

Batchelor, G.K., 1954. Heat transfer by free convection across a closed cavity between vertical boundaries at different temperatures. Quart. Appl. Math. 12, 209.

Betts, P.L., Bokhari, I.H., 1996. Experiments on turbulent natural convection of air in a tall cavity. Proceedings of the Fifth ERCOFTAC Workshop on Refined Flow Modelling, Chatou, France, April 1996.

Boomkamp, P., Boersma, B.J., Miesen, R., Beijnon, G., 1997. A Chebyshev collocation method for solving two-phase flow stability problems. J. Comp. Phys. 132, 191–200.

Boudjemadi, R., Maupu, V., Laurence, D., Le Quéré, P., 1997. Budgets of turbulent stresses and fluxes in a vertical slot natural convection at Rayleigh Ra = 10^5 and 5.410^5. Int. J. Heat and Fluid Flow 12, 70–79.

Chait, A., Korpela, S.A., 1989. The secondary flow and its stability for natural convection in a tall vertical enclosure. J. Fluid Mech. 200, 189–216.

Chapman, D.R., Kuhn, G.D., 1986. The limiting behaviour of turbulence near a wall. J. Fluid Mech. 170, 265–292.

D'afa alla, A.A., 1988. Turbulent Natural in a Tall Closed Cavity. PhD Thesis, University of Manchester, UK.

D'afa alla, A.A., Betts, P.L., 1990. Experiments on turbulent natural convection of air in a tall cavity. Proceedings of the Fifth ERCOFTAC Workshop on Refined Flow Modelling, Chatou, France, April 1996.

Dol, H.S., Hanjalić, K., Kenjeres, S., 1997a. A comparative assessment fo the second-moment differential and algebraic models in turbulent natural convection. Int J. Heat and Fluid Flow 18 (1), 4–14.

Dol, H.S., Hanjalić, K., 1997b. Development of a differential thermal second-moment closure using DNS-data of natural convection in a vertical channel. Addendum to the Second International Symposium on Turbulence, Heat and Mass transfer, Delft, pp. 31–40.

Dol, H.S., Hanjalić, K., Versteegh, T.A.M., 1998. The development of a differential thermal second-moment closure using DNS-data of natural convection in a vertical channel (to be submitted for publication).

Drazin, P.G., Reid, W.H., 1981. Hydrodynamic Stability, Cambridge University Press, Cambridge.

Elder, J.W., 1965a. Laminar free convection in a vertical slot. J. Fluid Mech. 23, 77–98.

Elder, J.W., 1965b. Turbulent free convection in a vertical slot. J. Fluid Mech. 23, 99–111.

Elder, J.W., 1966. Numerical experiments with free convection in a vertical slot. J. Fluid Mech. 24, 823–843.

Henkes, R.A.W.M., 1990. Natural-Convection Boundary Layers. PhD Thesis, Delft University of Technology, The Netherlands.

Ince, N.Z., Launder, B.E., 1989. On the computation of buoyancy-driven turbulent flows in rectangular enclosures. Int. J. Heat and Fluid Flow 10 (2), 110–117.

Komminaho, J., Lundbladh, A., Johansson, A.V., 1996. Very large structures in plane turbulent Couette flow. J. Fluid Mech. 320, 259–285.

Korpela, S.A., Gözüm, D., Baxi, C.B., 1973. On the stability of the conduction regime of natural convection in a vertical slot. Int. J. Heat and Mass Transfer 16, 1683–1690.

Mansour, N.N., Kim, J., Moin, P., 1988. Reynolds-stress and dissipation rate budget in a turbulent channel flow. J. Fluid Mech. 194, 15–44.

Nagano, Y., Yin, Y., Tsuji, T., 1989. Numerical prediction of turbulent buoyant flows. Seventh Symposium of turbulent shear flows.

Nieuwstadt, F.T.M., Versteegh, T.A.M., 1997. DNS of natural convection between two vertical, differentially heated walls. Eleventh Symposium on Turbulent Shear Flows, Grenoble.

Phillips, J.R., 1996. Direct simulations of turbulent unstratified natural convection in a vertical slot for $Pr = 0.71$. Int J. Heat and Fluid Flow 39 (12), 2485–2494.

Rotta, J.C., 1951. Statistische Theorie nichthomogener Turbulenz. Zeitschrift fur Physik 129, 547–572.

Rotta, J.C., 1972. Turbulente Strömungen. B.G. Teubner, Stuttgart.

Tsuji, T., Nagano, Y., 1988. Turbulence measurements in a natural convection boundary layer along a vertical flat plate. Int. J. Heat and Mass Transfer 31, 2101–2111.

Versteegh, T.A.M., 1998. Natural Convection in an Infinite, Differentially Heated, Vertical Channel. Ph.D. Thesis, Delft University of Technology (in preparation).

Vest, C.M., Arpaci, V.S., 1969. Stability of natural convection in a vertical slot. J. Fluid Mech. 36, 1–15.